12

ESO-891-B

LINE-STRENGTH GRADIENTS AND DYNAMICS OF NGC 2663 AND NGC 5018

C. Marcella Carollo and I. John Danziger

European Southern Observatory

Karl-Schwarzschildstraße 2, W-8046 Garching

Dec 1992

Presented at the ESO/EIPC Workshop on "Structure, Dynamics and Chemical Evolution of Early-Type Galaxies", Elba, Italy, 25-30 May 1992

ABSTRACT

Results of the analysis of long–slit spectra of NGC 2663 and NGC 5018 are presented. Mg_2, Fe_{5270} and Fe_{5335} line–strength gradients have been derived for both galaxies, together with rotation velocity and velocity dispersion curves at many position angles. These measurements extend to about 1.8 effective radii for NGC 2663, and to almost 3 effective radii for NGC 5018. NGC 2663 has a very steep velocity dispersion profile along the minor axis, and seems to have peculiar core kinematics; NGC 5018 shows a peculiarly flat velocity rotation curve, and is a good candidate for hosting dark–matter. Both its velocity dispersion and its Mg_2 line–strength profiles show a strong decrease in the center, the latter possibly indicating the existence of a merger–driven younger population. In both galaxies, the slopes of the iron line–strengths versus the Mg_2 index are, in agreement with the general trend shown by ellipticals, steeper than the slope followed by galactic nuclei.

1. INTRODUCTION

The introduction of new and more powerful instruments and observational techniques has led to enormous progress in understanding elliptical galaxies. They are more complex systems than previously thought, so that the distinction between them and lenticular galaxies may be more subtle than previously thought. Indeed stellar disks, which should be one of the decisive features in classifying a galaxy as lenticular, are often present in galaxies traditionally classified as ellipticals, and ellipticals with disky isophotes seem to be intrinsically similar to rotation–supported lenticular galaxies (Bender *et al.* 1989). The dynamical behaviour of some ellipticals – *i.e.* their rotation velocity and velocity dispersion profiles – can sometimes be modelled assuming that they are oblate rotators with only two integrals of motion, though

radial pressure anisotropy might be required (Binney, Davies, and Illingworth 1990, hereafter BDI; van der Marel, Binney and Davies 1990).

Recent studies of metallicity gradients inside ellipticals have also revealed unexpected features. Line–strength gradients seem to have a quite complex dependence on the mass of the galaxy (Carollo et al. 1992, hereafter CDBM), and they seem to indicate that the $[\frac{Fe}{Mg}]$ ratio is in general low relative to the solar ratio and much steeper inside galaxies than among galactic nuclei (see *e.g.* Faber, Worthey and Gonzales 1991; Davies, Sadler and Peletier 1992). There have also been suggestions (*e.g.* Bender et al. 1989; Bender 1991) that mergers causing the observed decoupled cores leave their signature also on the Mg_2 profiles, which show a change of slope at the radius of the core.

Despite the general progress, however, many aspects of the structure, dynamics, and formation of elliptical galaxies still remain very uncertain (see *e.g.* Kormendy and Djorgovski 1989; de Zeeuw and Franx 1991). Open issues such as the dark matter content or the star formation history of a galaxy can be investigated only by detailed studies of individual galaxies. Published line–strength gradients and kinematical quantities are till now mostly restricted to the inner regions of galaxies (*i.e.* inside one effective radius) and to only one position angle, although important information is contained in the profiles of the velocity and velocity dipersion curves at large radii , as well as in the profile of the metallicity indices at large radii.

In order to address these issues, we have concentrated our efforts on a small sample of early–type galaxies, which were studied in great detail by taking deep long–slit spectra at various position angles, and multicolour images. In this paper, we present the rotation velocity and velocity dispersion curves and the Mg_2, Fe_{5270} and Fe_{5335} line–strength profiles of two of the selected galaxies, namely NGC 2663 and NGC 5018. All these measurements extend well beyond the effective radii of the two galaxies. A more detailed discussion of the data presented here, together with the analysis of other unpublished spectra at different position angles and of broad–band multi–colour photometry of these two galaxies, will be published separately (Carollo and Danziger 1992, hereafter CD).

We give a brief summary on the properties of the two galaxies in Section 2, and an outline of the observations in Section 3. The kinematical profiles of the two galaxies are presented in Section 4, while the line–strength profiles are described in Section 5. A brief discussion of the results is given in Section 6.

2. THE TWO GALAXIES

The first object, NGC 2663, belongs to a sample of 42 galaxies for which we already had long–slit spectra, though not very deep. The analysis of such spectra has shown that this galaxy has a peculiarly high mass to light ratio when compared to the other objects in the sample (CDBM). It is a radio source, and shows strong [NII]6583 emission.

The second object, NGC 5018, has an anomalously low central metallicity for its luminosity, *i.e.* it deviates significantly from the fit to the Mg_2–σ relation followed by ellipticals nuclei (see *e.g.* Schweizer et al. 1990). It shows an irregular dust–lane, ripples and shells (see *e.g.* Schweizer, 1987), and has been considered a candidate for a merger remnant.

A brief review of the major parameters available from previous literature on these two galaxies is given in Table 1.

TABLE 1

Name	Type[1]	P.A.	Vel_{hel}	m_B	R_e	SB_e	ϵ	(B-R)	mg_2	σ_o
NGC 2663	S0/E	111	2130	11.9	50	23.5	.27	2.09	.324	281
NGC 5018	S0/E	99	2897	11.7	22	21.8	.28	1.41	.209	223

- The columns list: 1–name of the galaxy; 2–morphological type; 3–position angle of the major axis (NE); 4–heliocentric velocity; 5–apparent blue magnitude; 6–effective radius, *i.e.* half–light radius; 7–surface brightness at 1 effective radius; 8–ellipticity; 9– total (B-R) colour; 10–central value of mg_2 index; 11–central velocity dispersion.
- Units are: position angle of major axis in degrees; heliocentric velocity and velocity dispersion in Km/sec; effective radius in arcseconds; surface brightness at Re in mag/(arcsec)^2; central mg_2 and total (B-R) colour in magnitudes.
- All parameters are from the ESO Lauberts and Valentjin Catalog, with the exclusion of mg_2 and σ_o, which are from Davies et al. 1987.

[1] Both galaxies are classified as lenticulars in the ESO Lauberts and Valentijn Catalog, and as ellipticals in the RC3.

3. OBSERVATIONS

The long–slit spectra whose analysis is reported here were taken, using the red arm of EMMI at the ESO-NTT, on three nights from March 7 to March 9, 1992. The detector

characteristics and the instrumental setup are given in Table 2.

TABLE 2

Run	Telescope	Instrument	CCD[1]	ron	λ range	Slit[2]	Pixel Size[3]	Resolution
7–9 March	NTT	EMMI	ESO # 18	5	4700–5700	1.8	2×0.9	4.5

- Units are: read-out-noise (ron) in e^-/pixel; wavelength range in Å; slit width in arcseconds; pixel size in Å×arcseconds; resolution (*i.e.* FWHM of Thorium emission lines) in Å.

(1) Thomson Coated, 1024×1024 pixels of 19×19 μm^2.
(2) In table, the slit width. Its length was about 7 arcminuts.
(3) The CCD was rebinned 2×2; the listed pixel size already include such a rebinning.

To reduce cosmic–rays events on the CCD, the single exposures were limited to a maximum of one hour. The slit was always centered on the galaxy nucleus. Thorium calibration spectra were taken after each exposure to determine the wavelength scale.

Comparison stars, *i.e.* K giants and spectrophotometric standards, were also observed. The K giants, to be used as kinematical templates, were trailed across the slit, so to avoid the effects of mimicking of a narrower slit in case of good seeing and of atmospheric dispersion. The observing log for the galaxies and the calibration stars is given in Table 3.

TABLE 3

name[*]	P.A. (deg)	exposure time (sec)	Spectral Type
NGC 2663	111	6×3600	
NGC 2663	21	2×3600	
NGC 5018	99	5×3600	
NGC 5018	9	2×3600	
NGC 5018	54	1800+3600	
HR 2712			K2III
HR 2732			K2III
HR 6049			K2III
L745-46A			

(*) For each star, multiple exposures were taken.

The data were reduced using the ESO MIDAS system. A detailed description of the data reduction procedure is given in CD.

4. DYNAMICAL PARAMETERS

The kinematical profiles of NGC 2663 and NGC 5018 are shown respectively in Figs. 1 and 2.

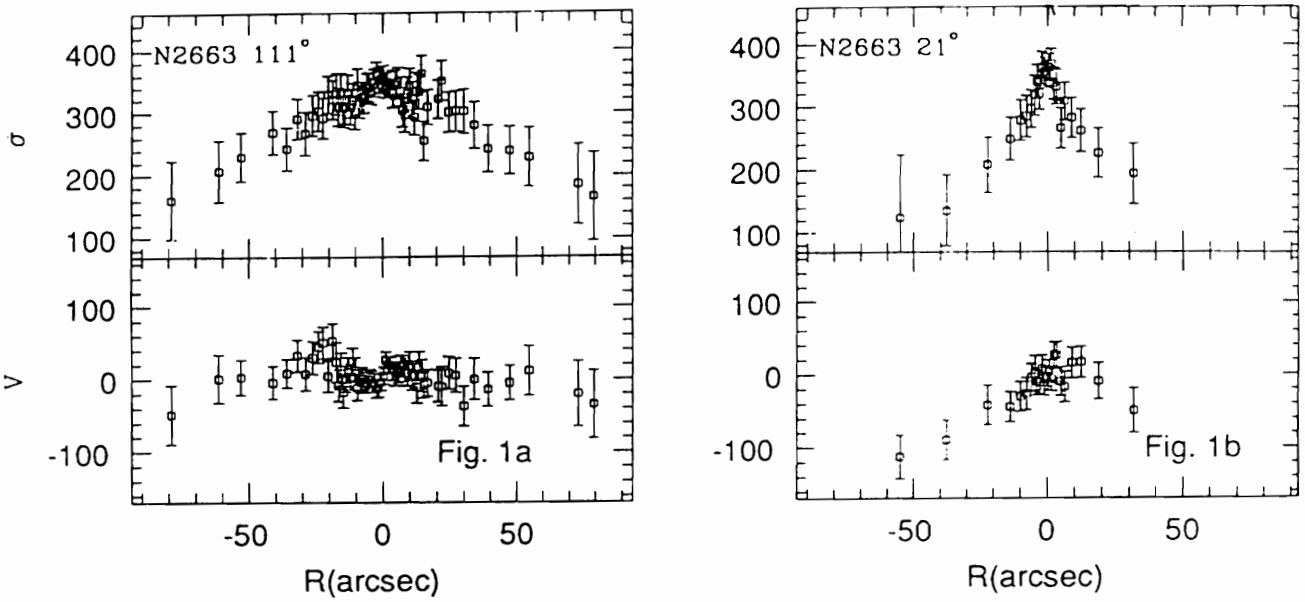

Fig. 1- Rotation velocity and velocity dispersion profiles of NGC 2663. In particular, Fig. 1a refers to major axis (*i.e.* P.A. 111°) and Fig. 1b to minor axis. The radius is in arcseconds.

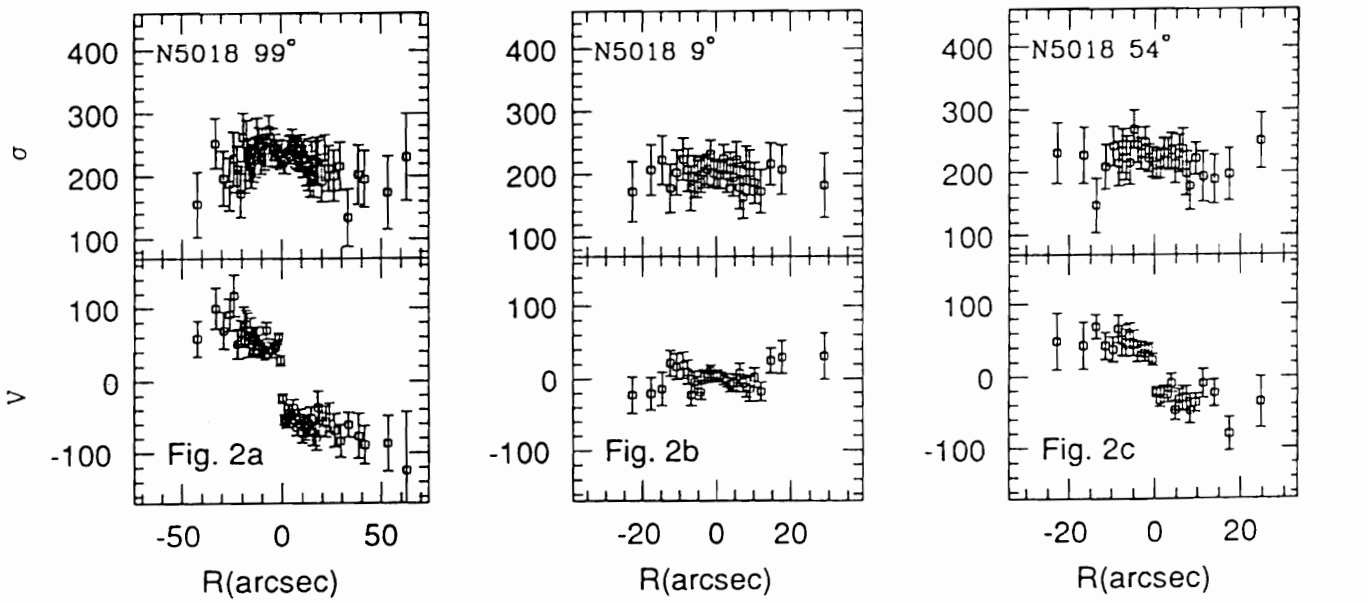

Fig. 2- Rotation velocity and velocity dispersion profiles of NGC 5018. In particular, Fig. 2a refers to major axis (*i.e.* P.A. 99°), Fig. 2b to minor axis and Fig. 2c to P.A. 54°. The radius is in arcseconds.

In particular, in Fig. 1a are plotted the rotation velocity and the velocity dispersion profiles relative to the major axis of NGC 2663 (*i.e.* P.A. 111°) and in Fig. 1b those relative to the minor axis. Similarly, Figs. 2a,b,c refer to major axis (*i.e.* P.A. 99°), minor axis and P.A. 54° of NGC 5018.

A Fourier Quotient package (Bertola et al. 1984) and, as a check, cross–correlation algorithms present in MIDAS were run on the fully reduced spectra. Results of the two methods are totally consistent. The rotation velocity and velocity dispersion profiles obtained by using different template stars were compatible within the errors.

5. LINE–STRENGTH PROFILES

The system of line–strengths of Burstein et al. (1984) was used to compute, on the de–redshifted spectra, radial line–strength gradients of Mg_2, Fe_{5270} and Fe_{5335}. The data presented here are not calibrated on the Lick System; the calibrated ones will be given in CD. Errors due to photon statistics for the continua and the absorption features themselves were computed according to Brodie and Huchra (1990).

Iron line–strengths were corrected for velocity dispersion broadening. The correction laws were derived convolving the available template spectra with gaussians mimicking values of sigma in the range 100–400 Km/s, averaging the results for different templates and fitting the obtained index–sigma average relations. Our velocity dipersion profiles, appropriately smoothed, were used to correct the iron indices on the whole radial range. At $\sigma \simeq 300$, these corrections were about 25% for Fe_{5270} and 50% for Fe_{5335}.

The line–strength profiles are shown in Figs. 3 and 4.

6. DISCUSSION

6.1 Kinematics and Dynamical Modelling

A signature of peculiar core kinematics is visible in the rotation curves of NGC 2663, expecially along the major axis. Along this axis, a relatively small "counter–rotation" seems in fact to be present inside the innermost 10 arcseconds, while no significant rotation is detected at larger radii. A modest rotation appears instead along the minor axis, which shows also a

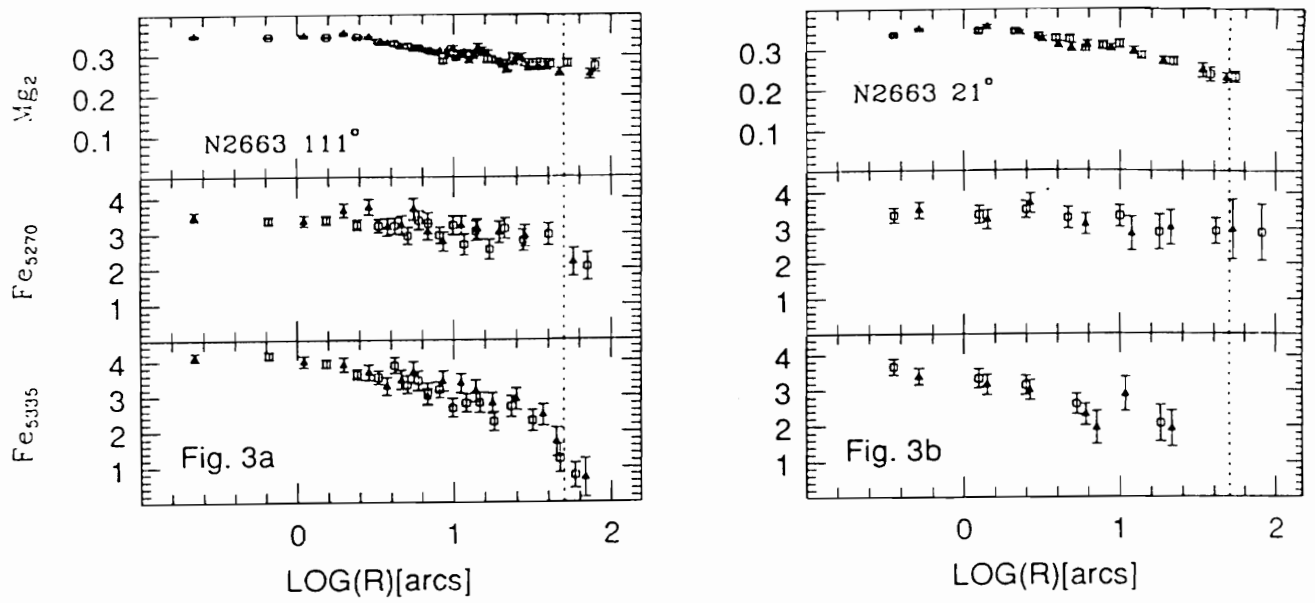

Fig. 3- Mg_2, Fe_{5270} and Fe_{5335} profiles for NGC 2663. In particular, Fig. 3a refers to major axis (*i.e.* P.A. 111°) and Fig. 3b to minor axis. The indices are plotted in function of Log_{10}(radius), in arcseconds. Mg_2 is in magnitudes and the iron lines in *Å*. Different symbols are used to distinguish the two opposite sides of the galaxy respect to the center. Vertical dashed lines are traced at 1 R_e.

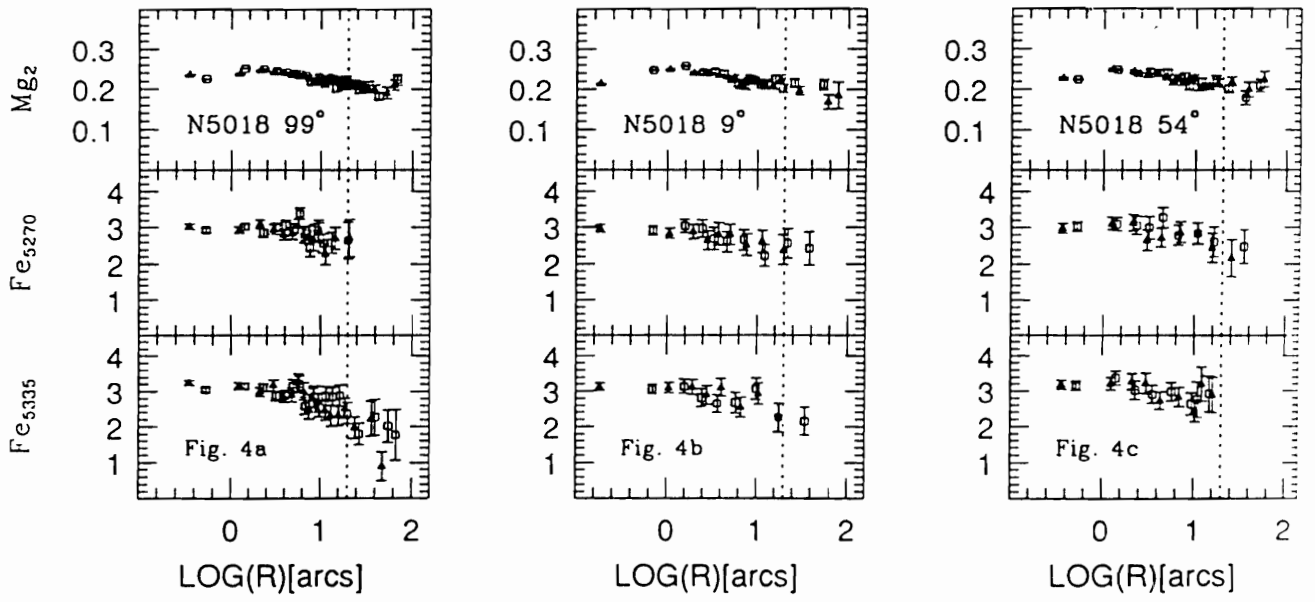

Fig. 4- Mg_2, Fe_{5270} and Fe_{5335} profiles for NGC 5018. In particular, Fig. 4a refers to major axis (*i.e.* P.A. 99°), Fig. 4b to minor axis and Fig. 4c to P.A. 54°. The indices are plotted in function of Log_{10}(radius), in arcseconds. Mg_2 is in magnitudes and the iron lines in *Å*. Different symbols are used to distinguish the two opposite sides of the galaxy respect to the center. Vertical dashed lines are traced at 1 R_e.

peculiarly steep velocity dispersion curve.

NGC 5018 is instead a fast–rotator along its major axis, without rotation on the minor axis. Along all three position angles shown here (and along a fourth one also, see CD), its velocity dispersion profile appears quite flat, even outside one effective radius. In addition, the velocity dispersion profile shows a peculiar decrease in the center, visible along the major axis.

In order to derive dynamical information from our data, we have attempted to model NGC 2663 and NGC 5018 as axisymmetric rotators, characterized by a distribution function depending only on the energy, E, and the angular momentum about the symmetry axis, J_z. We have adopted a simplified version of the modelling technique used by BDI, prompted by the fact that the light profiles of ellipticals are well–described by a Jaffe density law. We assume that the density of our galaxies is given in cylindrical coordinates, (R, z, ϕ), by:

$$\rho = \rho_0 \frac{1}{(1 + m/r_c)^2 (1 + m/r_m)^2}$$

with

$$m \equiv \sqrt{R^2 + \frac{z^2}{(1-\epsilon)^2}}.$$

Here r_c are r_m two scalelengths related, respectively, to the core and half–mass radii, while ϵ is the (constant) axial ratio.

Although the "natural" models are oblate rotators, prolate models are easily obtained by assuming the longest axis as the symmetry one.

In addition to the case of constant mass to light ratio, we have also considered the case where a dark massive halo is present. The dark halo is assumed to be diffuse and extended and is modelled as an isochrone Henon potential, with total mass M_D, scalelength r_D, and flattening ϵ_D. We have considered only spherical halos ($\epsilon_D = 0$), and halos with flattening equal to that of the stellar component ($\epsilon_D = \epsilon$). For each position angle we have projected the model data along a "simulated slit". Details of the modeling are given in CD.

We have then compared the observed velocity and velocity dispersion fields with the model predictions. Differently from BDI, no inversion is here involved, and it is then possible to determine the χ^2 of the fits. However, since the errors and the real number of statistically independent points in both the kinematic profiles and the light curve (published in CD) are

not easy to determine, we have used the χ^2 values mainly as a guide to determine the best models rather then as a measure of the statistical significance of our fits.

In the case of NGC 2663, only prolate models were explored, due to the presence of rotation along its minor axis. We were however not able to reproduce, within our family of models, the dynamical behaviour of this galaxy. This strongly suggests that this galaxy is a prolate rotator, but has strong radial anisotropy, or that it is an highly triaxial object.

A good fit to the rotation velocity and velocity dispersion profiles of NGC 5018 is instead given by an oblate rotator with a flattened, diffuse dark halo three times as massive as the luminous component. The insertion of the dark halo is necessary to fit the flat velocity dispersion curve of the galaxy along all three position angles which we sampled. Fig. 5 shows the best model compared with the data. From it, we derive a mass of $3\times10^{11}M_{\odot}$ for the luminous component, *i.e.* a luminous $\frac{M}{L_B}$ of about $6\frac{M_{\odot}}{L_{B\odot}}$.

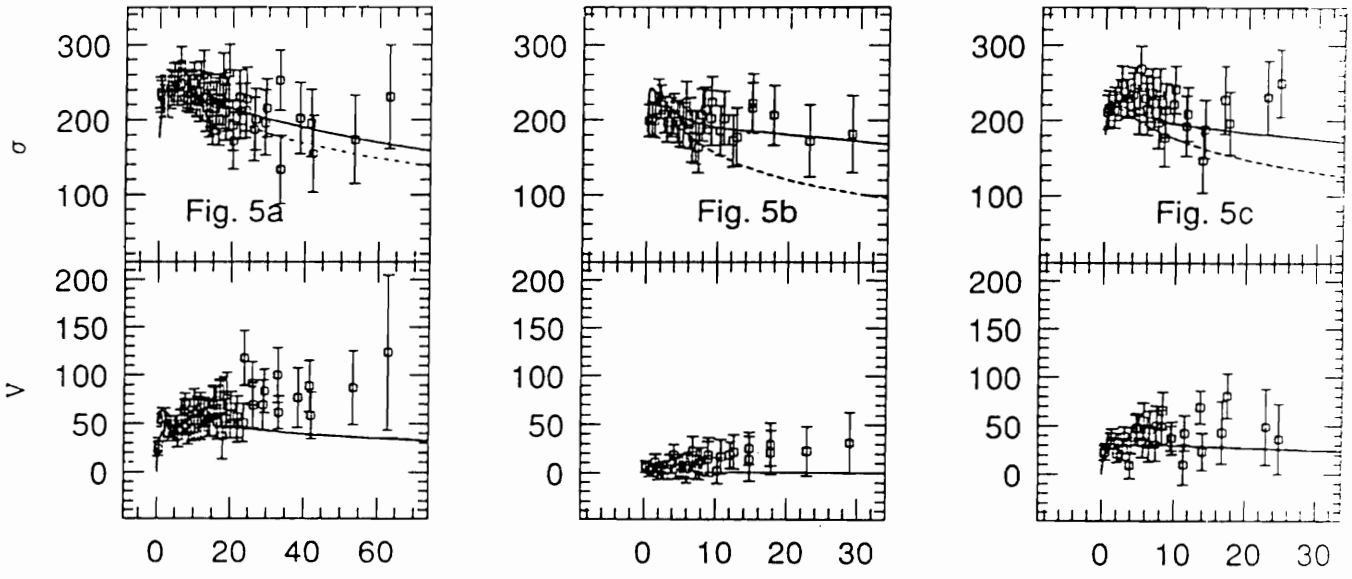

Fig. 5- The data of Fig. 2 are given, with the best–fit dynamical model for NGC 5018 overplotted (solid line), and the corresponding model without dark matter (dashed line). Parameters of the best–fit model are:

- inclination angle of the line of sight with the symmetry axis 60°;
- $M_D = 3\times M_{lum}$;
- $\epsilon_D = \epsilon_{lum}$
- $R_D = 4\times R_{lum}$;

6.2 The Metallicity Indices

The profiles of all the metallicity indices of NGC 2663 are relatively featureless, the only hint for some structure appearing in its Mg_2 profile at a distance of about 10–15 arcseconds from the center.

NGC 5018, instead, shows up as a quite peculiar galaxy also for its line–strength profiles. From our data, a strong decrease in its Mg_2 index is clearly visible at all three position angles corresponding to the σ decrease, *i.e.* inside an inner radius of about 2–3 arcseconds. This decrease is too large to be attributed to possible seeing effects. It seems as if, as suggested by *e.g.* Schweizer (1987), a merger–driven (?), younger population is causing the dilution of the Mg_2 index in that region. It is interesting to note that, if the Mg_2 profile were extrapolated from outer radii to the center, NGC 5018 would perfectly lie on the Mg_2–σ relation followed by ellipticals nuclei. Broad–band colour effects in the same region are being investigated (CD).

The central values and gradients of the line–strengths are listed, for both galaxies and separately for each position angle, in Table 4.

TABLE 4

Name	P.A.	Mg_2	Fe_{5270}	Fe_{5335}	$-\frac{dMg_2}{dlogr}$	$-\frac{dFe_{5270}}{dlogr}$	$-\frac{dFe_{5335}}{dlogr}$
NGC 2663	111	.347(.003)	3.45(.13)	3.94(.19)	.060(.002)	.33(.07)	.97(.06)
NGC 2663	21	.343(.007)	3.43(.13)	3.31(.22)	.074(.005)	.23(.13)	.91(.17)
NGC 5018	99	.240(.001)	2.97(.07)	3.13(.08)	.038(.002)	.10(.06)	.42(.05)
NGC 5018	9	.239(.002)	2.92(.09)	3.06(.08)	.035(.004)	.23(.08)	.29(.09)
NGC 5018	54	.237(.010)	3.06(.05)	3.21(.08)	.033(.004)	.20(.10)	.28(.11)

- Units are: position angle in degrees; Mg_2 in magnitudes; two iron lines in $\AA$; the Mg_2 and the iron slopes respectively in mag/dex and $\AA$/dex.
- 1-σ errors are given in parenthesis. They are defined as rms of averaged points for central values. Formal errors of the fits are given for the gradients.

For both galaxies, Mg_2 gradients have been obtained excluding the points in the innermost 2.5 arcseconds. All the available data were instead considered when fitting the Fe line profiles.

In Figs. 6 we plot, for both NGC 2663 and NGC 5018, the average iron <Fe> (*i.e.* $\frac{1}{2}(Fe_{5270}+Fe_{5335})$) versus the Mg_2 index. Also plotted there is the line corresponding to the slope followed by the galactic nuclei, taken from Burstein et al. (1984).

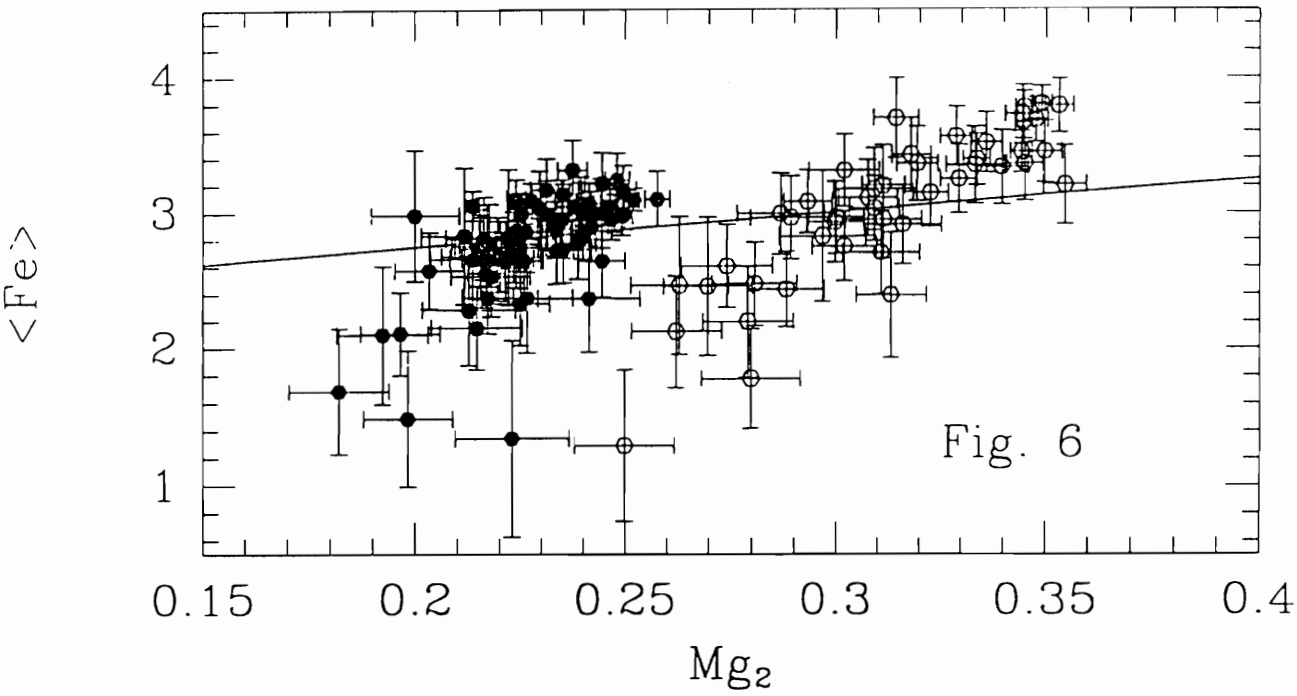

Fig. 6- <Fe> versus Mg_2 for NGC 2663 (open symbols) and NGC 5018 (filled symbols). Mg_2 is in magnitudes and the iron lines in $\AA$. Overplotted is the fit to the galactic nuclei, taken from Burstein et al. (1984).

Our data indeed confirm that ellipticals show an internal <Fe> *vs.* Mg_2 slope steeper than the one followed by their nuclei. The two internal slopes of NGC 2663 and NGC 5018 are very similar, and both consistent with the slope of models of stellar populations with constant $[\frac{Mg}{Fe}]$ (slope $\simeq$ 8; see Peletier 1989; Davies, Sadler and Peletier 1992). The two galaxies show however very different values of <Fe> around $Mg_2 \simeq 0.25$. The two profiles are consistent with a scenario in which the $[\frac{Mg}{Fe}]$ ratio remains constant inside ellipticals, but varies from galaxy to galaxy. In particular, the observed indices ratio in NGC 2663 implies, in agreement with the general behaviour shown by giant ellipticals (see *e.g.* Davies, Sadler and Peletier 1992), an $[\frac{Mg}{Fe}]$ abundance ratio higher than solar. The observed $[\frac{Mg_2}{<Fe>}]$ profile in NGC 5018, instead, lies above the models for solar ratio; no other giant elliptical among those studied untill now shows this feature. Why this galaxy occupies this peculiar position on the Mg_2-

<Fe> plane is still unclear; future similar studies on other "merger remnants", compared to "normal" ellipticals, might help in finding an answer. This will require detailed modelling of stellar populations.

Acknowledgements

We are grateful to M. Stiavelli for his essential help in implementing the modified version of BDI's dynamical modelling program, and in the computation of the models presented in this paper. We also wish to thank R. Peletier and P.T. de Zeeuw for many stimulating comments on an earlier version of this paper. C.M.C. wishes to thank F. Matteucci, R. Peletier, M. Stiavelli and W. Zeilinger for innumerable elucidating discussions.

REFERENCES

Bender, Surma, Döbereiner, Möllenhof and Madejsky, 1989, *A. A.* **217**, 35.

Bender, 1991, *IAU Symp.* **149**, 267.

Bertola, Bettoni, Rusconi and Sedmak, 1984, *A. J.*, **89**, 356.

Binney, Davies, and Illingworth, 1990, *Ap. J.* **361**, 78 (BDI).

Brodie and Huchra, 1990, *Ap. J.* **362**, 503.

Burstein, Faber, Gaskel and Krumm, 1984, *Ap. J.* **287**, 586.

Carollo and Danziger, 1992, *in preparation* (CD).

Carollo, Danziger, Buson and Matteucci, 1992, *in preparation* (CDBM).

Davies, Sadler and Peletier, 1992, *submitted to M.N.R.A.S.*.

de Zeeuw and Franx, 1991, *Ann. Rev. Astr. Astroph.* **29**, 239.

Faber, Worthy and Gonzales, 1991, *IAU Symp.* **149**, 255.

Franx and Illingworth, 1990, *Ap. J. Lett.* **359**, L41.

Kormendy and Djorgovski, 1989, *Ann. Rev. Astr. Astroph.* **27**, 235.

Peletier, 1989, *Ph. D. Thesis*, Groeningen

Schweizer, 1987, *IAU Symp.* **127**, 109.

Schweizer, Seitzer, Faber, Burstein, Dalle Ore and Gonzales, 1990, *Ap. J. Lett.* **364**, L33.

van der Marel, Binney and Davies, 1990, *M. N. R. A. S.* **245**, 582.